Wiley
Shock and Vibration
Volume 2024, Article ID 5060571, 13 pages
https://doi.org/10.1155/2024/5060571

WILEY

Research Article

Study on Ultrasonic Characteristics and Prediction of Rock with Different Pore Sizes

Lei Wang[1,2] **Wen Nie**[1] **Ming Xie**[3] **Zi Wang**[1,3] **Wei Lu**[4] **Dongmei Chen**[5] **and Weinan Lin**[2]

[1]*Quanzhou Institute of Equipment Manufacturing, Haixi Institutes, Chinese Academy of Sciences, Quanzhou 362201, China*
[2]*College of Civil Engineering, Ludong University, Yantai 264025, China*
[3]*College of Civil Engineering, Xijing University, Xi'an 710123, China*
[4]*Research Center of Geotechnical and Structural Engineering, Shandong University, Jinan 250061, China*
[5]*Jinjian Engineering Design Limited Company, Yantai 264000, China*

Correspondence should be addressed to Wen Nie; wen.nie@fjirsm.ac.cn

Received 26 April 2023; Revised 16 March 2024; Accepted 12 April 2024; Published 23 May 2024

Academic Editor: Carlo Rosso

The internal defects of rocks are the main cause of instability and failure in underground engineering. Therefore, using ultrasonic monitoring technology to study the defect characteristics of rocks containing voids is of great significance. The research results indicate that with the increase in the pore size, the longitudinal wave velocity and first wave amplitude of rocks containing voids decrease, the attenuation coefficient increases, and the difference in ultrasonic parameters between rocks containing voids and intact rocks increases, resulting in a significant decrease in the rock integrity. The propagation of ultrasonic waves in porous rocks can be divided into three stages, where obvious ultrasonic reflection, diffraction, and scattering occur. The attenuation of sound pressure is significant, and the ultrasonic sound pressure is negatively linearly correlated with the pore size. Based on the amplitude, velocity, and pressure of ultrasonic waves, an ANN-based method for predicting the pore size of rocks is proposed, which inverts and predicts the pore size of rock masses with high prediction accuracy.

1. Introduction

China's economy has shifted from a stage of rapid growth to a set of high-quality development. Infrastructure is the basis for the high-quality development of the national economy. It has also become an essential support for transforming new and old driving forces in the new era. National strategies such as the "Asian Investment Bank" and the "Belt and Road" focus on infrastructure construction. Infrastructure industries such as water conservancy, transportation, municipal administration, and mining have entered unprecedented development. As the buried depth of the tunnel increases, the stress increases, and the environment in which the rock mass is located becomes more complex [1]. The frequency and intensity of rock mass disasters significantly increase, seriously affecting the safe construction of the tunnel and threatening the safe operation of the tunnel [2, 3].

As the primary solid medium in tunnel engineering, rock's stability directly affects tunnel engineering's safety. During the excavation process of a tunnel, the excavation unloading effect affects the rock. A large number of cracks and holes are generated in the tunnel rock, resulting in anisotropy and heterogeneity of the rock, causing damage to the rock mass, and affecting the tunnel's safety. However, internal defects in the rock can cause changes in acoustic parameters [4–7]. Ultrasonic monitoring is often used to detect the integrity of the rock. Therefore, an in-depth research is conducted on identifying and predicting rock hole characteristics [8–15]. It is of great significance to guide the construction of tunnel engineering and the prevention and prognosis of geotechnical engineering geological disasters.

Many foreign scholars have conducted relevant research. Liu et al. [16] used a self-developed dry-coupled rock ultrasonic monitoring system to study the changes in P-wave

and S-wave during the stress process of granite. Nie et al. [17] used second harmonic generation technology to detect mortar contact type defects, obtained the relationship between excitation voltage and c, and obtained the crack length. Kurtulus et al. [18] conducted experiments on the influence of parallel and variable joints on ultrasonic pulse propagation in two 60 mm × 60 mm × 360 mm colourful marble blocks with no joints, six similar joints, and six unstable joints. The relationship between the number of joints and ultrasonic pulse velocity is analysed statistically. The relationship between the number of joints and ultrasonic pulse velocity was statistically analysed. Baechel [19] showed that the size and porosity of pores in rock masses can affect the elastic properties of carbonate rocks, indicating that the smaller the pore size, the better the correlation with wave velocity. Research by Mritunjay [20] shows that when the hole size is smaller than the wavelength, the sensitivity of acoustic waves to hole size changes is very low and can be ignored. Hevin et al. [21] studied the effect of crack shape on surface wave propagation. They established a corresponding relationship between the synthesised surface wave signal and the change in crack depth so the actual crack depth can be calculated through the complementary relationship between the fundamental wave signals.

The above research has analysed the ultrasonic parameter variation characteristics of internal fractures and joints in rock, which has a significant reference value. However, it has yet to explore the ultrasonic aspects of rock-containing voids and use ultrasonic characteristics to predict rock voids. Given this, this article takes red sandstone as the research object, analyses the ultrasonic elements of rock under different pore diameters, and uses ultrasonic parameters to predict rock pore diameters, providing a theoretical basis for rock stability analysis.

2. Ultrasonic Testing Scheme for Rock with Holes

The rock sample used for the test is red sandstone. Rock samples with uniform texture are collected on-site.The rock samples collected are precisely cut and polished in the laboratory to achieve a relatively flat surface for the creation of standard test pieces, measuring 100 mm × 100 mm × 100 mm. Defect-free rock samples are chosen, and drill bits of varying diameters including 10 mm, 15 mm, 20 mm, 25 mm, and 30 mm are selected to bore into the test pieces. Drill goes through the test specimen to a depth of 100 mm. There are five groups of rock samples with different hole sizes, and select 1 group of complete samples as the control group, as shown in Figure 1.

Using rock mechanics test instruments, the mechanical properties of red sandstone are tested on complete red sandstone specimens, and the mechanical parameters of red sandstone are obtained; they are given in Table 1.

The test uses the HS-YS2A rock acoustic wave testing system produced by Tianhong Electronics Research Institute, which mainly includes the ultrasonic transmitting device, receiving device, ultrasonic transducer, and data collector. The instrument comes with 250 V and 1000 V transmission pulse voltages, with a transmission pulse width of 0.2 to 100 μ adjustable, the gain range is 0.01–8000 times, the bandwidth range is 10 Hz–200 kHz, and the instrument adopts the current advanced industrial control computer, which can perform single acquisition and continuous acquisitions.

Apply Vaseline to the centre of the left and right sides of the sample, with an area larger than the cross-sectional area of the transducer. Place the transducer on both sides of the sample, and apply an appropriate amount of pressure to both sides of the transducer to fully contact the rock sample with the transducers on both sides. Click the acquisition button to start collecting the waveform, and then, adjust the magnification to make the waveform clear and complete, collecting the wave speed and amplitude as shown in Figure 2.

3. Test Results and Discussion

3.1. Variation Law of Ultrasonic Wave Velocity in Rock with Holes. To quantitatively compare the integrity of rock-containing voids, define the integrity of rock-containing holes, ξ, by

$$\xi = \left(\frac{v_k}{v_w}\right)^2. \tag{1}$$

Table 2 and Figure 3 show that

(1) With the increase in the rock pore diameter, the longitudinal wave velocity of rock-containing holes presents a downward trend. When the rock pore diameter increases from 10 mm to 30 mm, the ultrasonic wave velocity decreases from 2330 m/s to 2243 m/s, a decrease of 3%. The rock pores reduce the ultrasonic wave velocity.

(2) As the pore diameter of the rock increases, the difference between the longitudinal wave velocities of porous rock and intact rock tends to increase. When the pore diameter is 10 mm, 15 mm, 20 mm, 25 mm, and 30 mm, the longitudinal wave velocities of porous rock decrease by 4%, 4.37%, 4.10%, 5.46%, and 6.93%, respectively, and the rate of change of longitudinal wave velocity before and after generally presents an increasing trend. However, based on the overall analysis, the attenuation of ultrasonic longitudinal wave velocities is small, and the size of the hole has little impact on the first wave velocities; the main reason is that when there is a porous medium in the rock mass, ultrasonic waves will diffract around the hole, cutting off the central propagation path and increasing the course. However, the propagation paths on both sides of the hole can be reached normally, and the arrival time of the first wave is consistent with the complete rock sample.

(3) As the pore diameter of rock increases, the integrity of rock-containing voids is negatively proportional to the pore diameter. When the pore diameter increases from 10 mm to 30 mm, the integrity of rock-containing holes decreases from 0.92 to 0.89, significantly reducing the integrity of the rock.

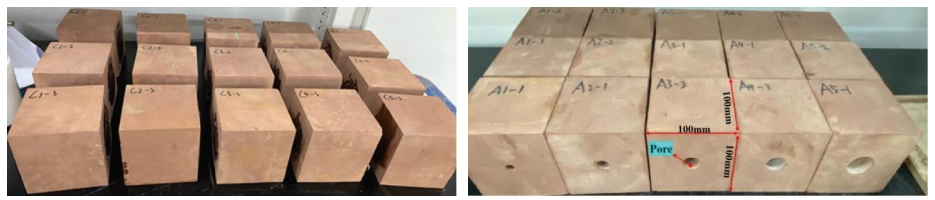

Figure 1: Rock sample specimen.

Table 1: Mechanical parameters of red sandstone.

UCS (MPa)	Elastic (GPa)	Deformation (GPa)	μ	Density (g/cm^3)
85.43	6.79	3.45	0.325	2.51

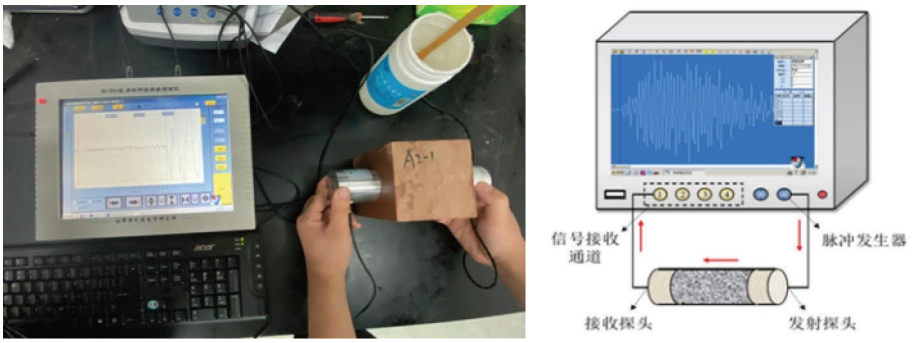

Figure 2: Test process.

Table 2: Variation of the attenuation coefficient of rock samples with different pore sizes before and after drilling at 100 kHz.

Rock sample number	Aperture size (mm)	Longitudinal wave velocity before drilling (m/s)	Longitudinal wave velocity after drilling (m/s)	Wave velocity difference (m/s)
A1	10	2427	2330	97
A2	15	2428	2322	106
A3	20	2414	2315	99
A4	25	2417	2285	132
A5	30	2410	2243	167

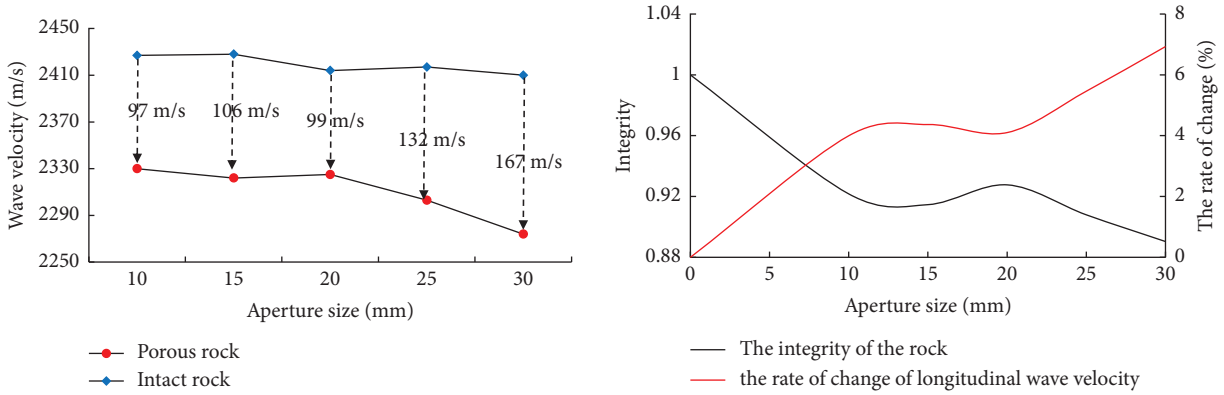

Figure 3: Changes in the ultrasonic wave velocity of rocks with different apertures.

3.2. Variation Law of Ultrasonic Wave Amplitude and Attenuation in Rock with Holes. The rock acoustic wave testing system is used to conduct ultrasonic testing on rock samples with circular holes with pore sizes of 10 mm, 15 mm, 20 mm, 25 mm, and 30 mm, respectively, and collect the first wave amplitudes of different pore sizes at a testing frequency of 100 kHz.

Table 3 and Figure 4 show that

(1) With the increase in the pore size, the amplitude of the first wave in rock-containing voids tends to decrease, with the pore size increasing from 10 mm to 30 mm and the amplitude of the ultrasonic first wave decreasing from 394 mv to 295 mv, a decrease of 25%. The difference between the amplitude of the first wave in porous and intact rock is positively proportional to the aperture. The attenuation amount and rate of the first wave amplitude increase with the aperture increase. When the aperture is 10 mm, 15 mm, 20 mm, 25 mm, and 30 mm, the attenuation rates of the first wave amplitude in porous rock are 10.86%, 15.26%, 21.85%, 24.94%, and 31.71%, respectively.

(2) When the hole size is between 10 mm and 30 mm, there is a linear correlation between the hole size and the amplitude of the first wave. Based on the optimal fitting curve of the aperture D-amplitude F, the relationship between the amplitude of the first wave F and the aperture D is obtained as $F = -4.4786D + 433.32$. Therefore, it is possible to predict whether there is a hole defect inside the rock mass by increasing and decreasing the amplitude of the first wave.

Read the amplitude of the first wave of the incident wave and the transmitted wave. Use the signal comparison method to calculate the ultrasonic attenuation coefficient of rock samples with different aperture sizes, as given in Table 4:

$$\delta = \frac{(\ln A_0 - \ln A)}{L}, \tag{2}$$

where A_0 is the first wave amplitude of the incident waveform, A is the first wave amplitude of the transmitted waveform, and L is the length of the sample.

The relationship between the attenuation coefficient and pore diameter of rocks with different holes is shown in Figure 5. It can be seen that the attenuation coefficient increases with the increase in the pore diameter and assumes a linear relationship. When the pore diameter is small, the difference in the attenuation coefficient between rocks with holes and intact rocks is slight. When the pore diameter is large, the attenuation coefficient between rocks with holes and entire rocks becomes larger and larger. When the pore diameter of rock increases from 10 mm to 30 mm, the attenuation coefficient increases from 22.9 dB/m to 25.8 m/s, an increase of 12.7%. The main reason is analysed: when ultrasonic waves propagate through holes and defects in the rock mass, at the boundary of the defect medium, due to diffraction, reflection, and scattering phenomena, the acoustic energy begins to attenuate. As the pore size increases, the higher the internal porosity of rock mass, the more severe the energy attenuation, and the higher the attenuation coefficient.

4. Study on Ultrasonic Propagation Characteristics in Rock with Holes

4.1. Establishment of Numerical Model. The numerical calculation uses the sound pressure transient module in COMSOL Multiphysics software to simulate the propagation of ultrasonic waves in three-dimensional porous media. The numerical calculation is used to analyse the propagation law and sound pressure distribution characteristics of ultrasonic waves in three-dimensional porous media and the specific analysis of the impact of hole size on the sound pressure transmission coefficient and signal spectrum characteristics.

Numerical calculation model width × high × thick is 100 mm × 100 mm × 100, taking the aperture size as a variable, and seven models with an aperture of 0 mm to 30 mm are established. The model is divided into a freely dissected tetrahedral mesh with good adaptability, using a 100-kHz Gaussian pulse as an excitation signal and a generalised α time step algorithm, as shown in Figure 6.

The specific methods for numerical simulation are as follows:

(1) Based on the physical experimental model, it selects a physical field in COMSOL Multiphysics software, adds a physical field interface, defines the solution type, and establishes a 3D model in the geometric functional area.

(2) It defines material properties in the solution domain, divides grid elements, and sets sound field boundaries and sound wave excitation sources.

(3) It solves the time-domain transient calculation of the model and extracts and processes the acoustic signal.

4.2. Analysis of Ultrasonic Propagation Characteristics of Rock with Holes

4.2.1. Analysis of the Influence of Transmitted Wave Signals on Rocks with Holes. Ultrasonic signals are emitted from the upper boundary of the model, and boundary probes are set at the left and lower limits of the model. The effect of different hole sizes on transmitted wave signals is studied by extracting and analysing boundary probe data. As shown in Figure 5, the transmission signal effect diagram of varying hole size models is used to compare and analyse the transmission signals of the 0 mm hole model and different hole size models.

As shown in Figure 7, the waveform signals received by the 0 mm to 30 mm hole model at the boundary are all a complete cycle, and the transmitted signals of different models start to jump simultaneously. By zooming in, it can be found that the time for each group of models to reach the

Table 3: Amplitude of the first wave before and after drilling of rock samples with different pore sizes at 100 kHz.

Rock sample number	Aperture size (mm)	Head wave amplitude before drilling (mv)	Head wave amplitude after drilling (mv)	Amplitude difference (mv)
A1	10	442	394	48
A2	15	426	361	65
A3	20	444	347	97
A4	25	433	325	108
A5	30	432	295	137

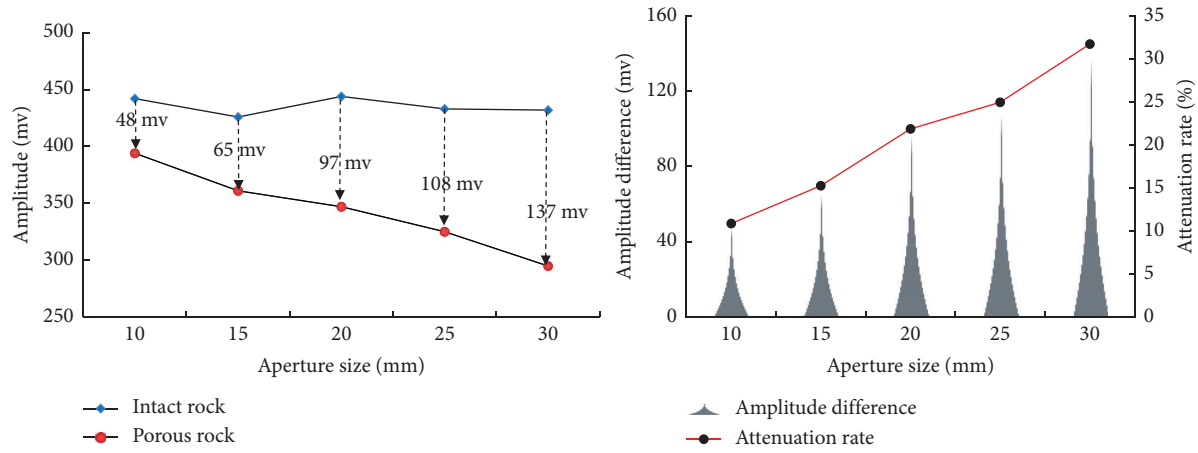

Figure 4: Wave amplitude variation of rocks with different apertures.

peak is different, but the difference is negligible. The time point for getting the rise is delayed from the 0 mm hole model to the 30 mm hole model. The model with a hole size of 0 mm is approximately 54.2 μs, and the sound pressure reaches its peak point; the model with a hole size of 30 mm is about 54.4 μs, and the sound pressure reaches its peak point. The sound time is delayed by 0.2 μs. This indicates that the hole size gradually increases, and the acoustic velocity does not significantly change. The simulation results agree with the experimental results, and the sensitivity of the wave velocity to the change in the hole size is relatively low.

4.2.2. Analysis of the Influence of Acoustic Pressure Attenuation Law on the Rock with Holes. As can be seen from Figure 8, the transmission boundary acoustic pressure amplitude has a negative linear correlation with the aperture. In contrast, the acoustic pressure amplitude reduction rate positively correlates with the aperture. The maximum amplitude of the sound pressure wave for a 0 mm complete model is 669.20 Pa. The acoustic pressure wave amplitudes of the 5 mm, 10 mm, 15 mm, 20 mm, 25 mm, and 30 mm hole models are 655.30 Pa, 620.20 Pa, 584.50 Pa, 549.20 Pa, 515.10 Pa, and 482.20 Pa, respectively, which are 2.08%, 7.32%, 12.66%, 17.93%, 23.03%, and 27.94% lower than those of the complete model. When the hole size is 30 mm, the impact of acoustic wave propagation is most evident. The apparent reason for analysis is that the acoustic wave undergoes various phenomena such as reflection, scattering, and diffraction; this causes attenuation of acoustic energy at the receiving boundary, resulting in a decrease in the wave amplitude. It has also been verified that using ultrasonic waves to detect hole defects has a good effect.

Ultrasonic waves propagate in the form of energy. When bearing in two different media, the energy of acoustic waves will attenuate. In order to conduct a quantitative analysis of the attenuation properties of ultrasonic waves in porous rocks, this study introduces a key parameter: the amplitude transmission coefficient, denoted as α. The more significant the transmission of ultrasonic waves in the model, the smaller the attenuation of ultrasonic energy.

$$\alpha = \frac{A_i}{A_o}, \tag{3}$$

where α is the amplitude transmission coefficient, A_i means different hole models receive signal amplitudes, A_o means the complete model receives the signal amplitude.

As seen in Figure 9, the ultrasonic amplitude transmission coefficient decreases linearly with the aperture increase. The transmission coefficient of the complete model is 1. When the aperture increases from 5 mm to 30 mm, the transmission coefficient decreases from 0.98 to 0.72, with a reduction rate of 26%. This indicates that the size of the hole is crucial to the transmission of ultrasonic sound waves. The larger the hole size, the more significant the impact of acoustic transmission ability and the more severe the attenuation of acoustic energy. Due to the physical test results of acoustic wave testing on rock samples with different hole sizes, the amplitude of the first wave gradually decreases as the hole size increases, and the conclusions obtained from numerical simulation are consistent with the test.

Table 4: Attenuation coefficient before and after drilling of rock samples with different pore sizes at 100 kHz.

Rock sample number	Aperture size (mm)	Attenuation coefficient before drilling (dB/m)	Attenuation coefficient after drilling (dB/m)	Attenuation coefficient difference (dB/m)
A1	10	21.7	22.9	1.1
A2	15	22.1	23.8	1.7
A3	20	21.7	24.2	2.5
A4	25	21.9	24.8	2.9
A5	30	22.0	25.8	3.8

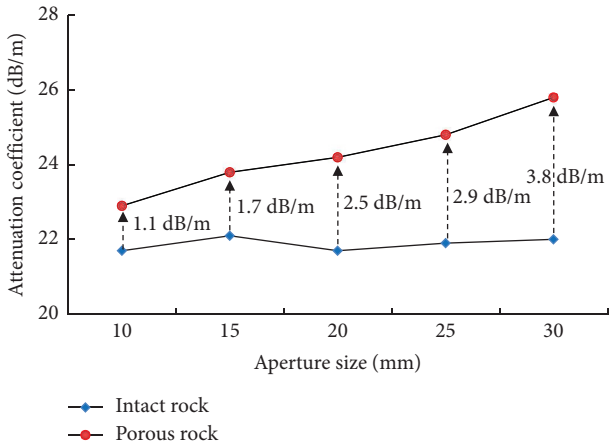

Figure 5: Variation of the attenuation coefficient of rocks with different apertures.

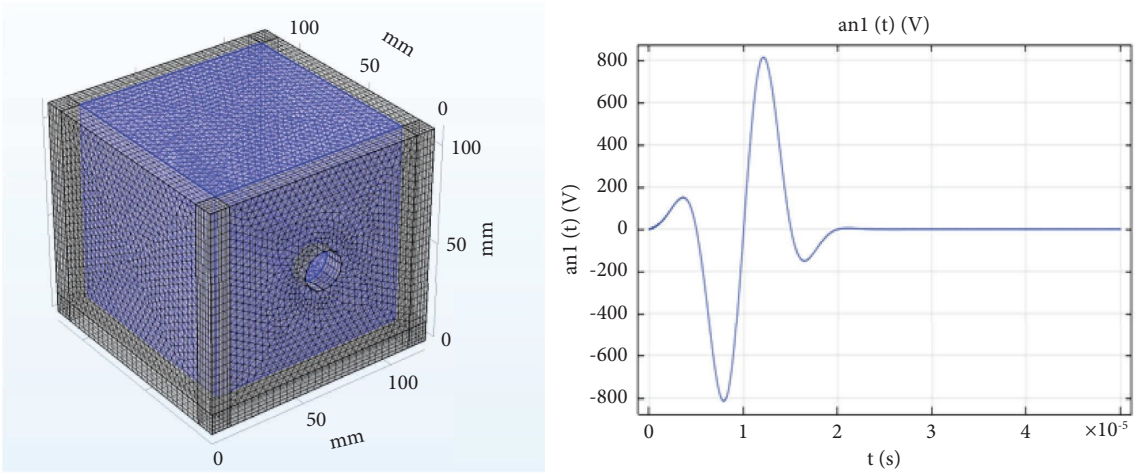

Figure 6: Numerical calculation model.

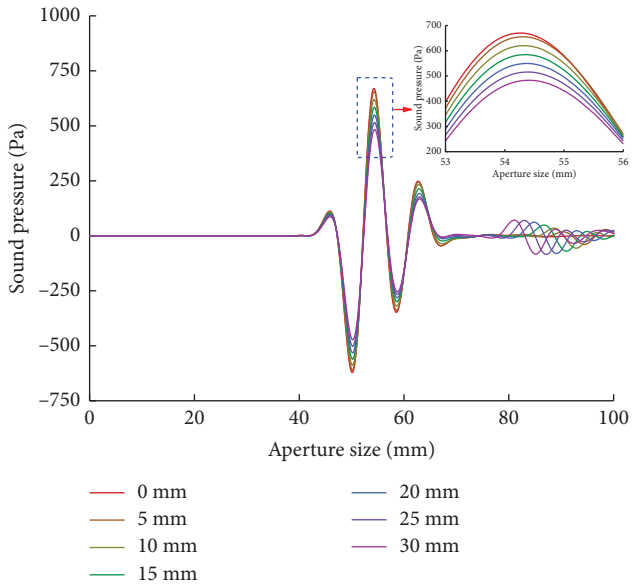

Figure 7: Comparison of transmission signals of different hole size models.

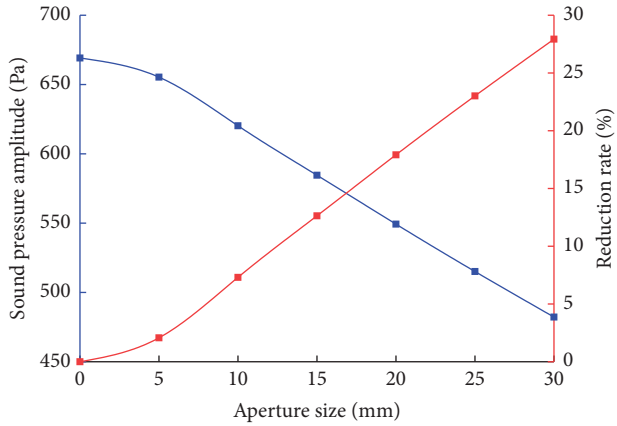

Figure 8: Diagram of the relation between the wave amplitude and hole size.

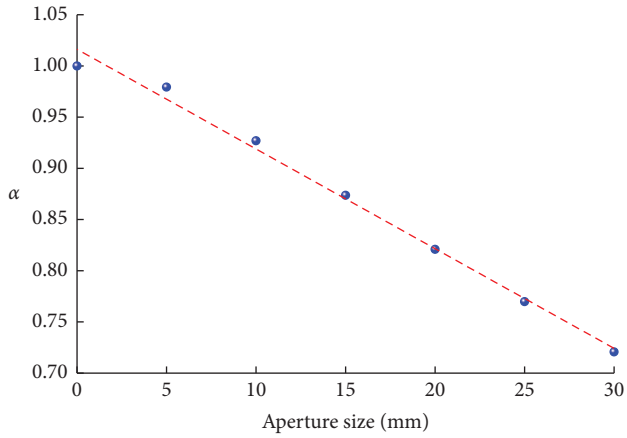

Figure 9: Relationship between the amplitude transmission coefficient and the hole size.

4.2.3. Acoustic Pressure Distribution Characteristics of Rock with Holes. To investigate the acoustic pressure distribution characteristics within rocks, this research initiates a 100 kHz ultrasonic signal at the model's upper boundary. This study aims to examine the variations in acoustic pressure over different time intervals and aperture sizes. Figure 10 shows the acoustic pressure distribution characteristics of the 20 mm hole model at other times, and Figure 11 shows the sound pressure contour surface of different hole models at the same time (70 μs). According to the distribution of sound pressure and the size of sound pressure, the sound pressure in the process of ultrasonic propagation in different hole size models is analysed.

As can be seen from Figure 10, the propagation of ultrasonic waves in porous rocks is divided into three stages: the first homogeneous propagation stage: this stage starts from the upper boundary to the time when the acoustic waves reach the edge of the hole, propagating downward at a certain sound pressure, and the sound pressure decreases. The second hole propagation stage: In this stage, ultrasonic waves pass through the hole, and apparent emission and transmission phenomena occur in the hole. The sound pressure at the edge of the hole fluctuates, forming a sound pressure rising region. The third stage is the propagation stage after the hole. In this stage, after the ultrasonic wave passes through the hole, apparent ultrasonic diffraction and scattering phenomena occur, and the sound pressure attenuates significantly.

Given the model's variations in hole sizes, the equivalent surface for sound pressure is correspondingly different. At 70 μs, the propagation of ultrasonic waves in the rock is in the third stage. When the ultrasonic waves reach the lower boundary, due to the influence of the pores, phenomena such as diffraction, reflection, and scattering occur. The change in sound pressure at this time can better reflect the influence of the pore size. Therefore, when the sound wave reaches 70 μs, the sound pressure equivalent surface of varying hole size models is extracted. At the same time, due to the different hole sizes, the distribution of the acoustic pressure isosurface of this group of models is also not the same. With the increase in the hole size in the model, the larger the cross-sectional area of the hole defect, the lower the acoustic pressure gradually.

5. Prediction of Hole Size Based on Acoustic Parameters

5.1. Data Enhancement. According to the results of indoor experiments and numerical calculations, there is a negative linear correlation between the ultrasonic amplitude and sound pressure and aperture, with a correlation coefficient of 0.95–0.99, which has a good correlation. To more accurately reflect the regularity and correlation between the rock pore size and sound pressure, amplitude, and wave velocity, adding more samples and enhancing the dataset are necessary. According to the correlation function, the 100 mm × 100 mm × 100 mm rock sample pore size is increased to 80 mm. The test amplitude and simulated sound pressure are obtained under different pore size conditions, as shown in Figure 12.

The relationship between the wave velocity and aperture is relatively complex and does not have clear rules. Therefore, an SVR-based wave velocity prediction model is established [22]. The dataset includes amplitude and sound pressure data for three model sizes, with model size, amplitude, and sound pressure as input values and wave velocity as output values. The predicted wave velocity value is

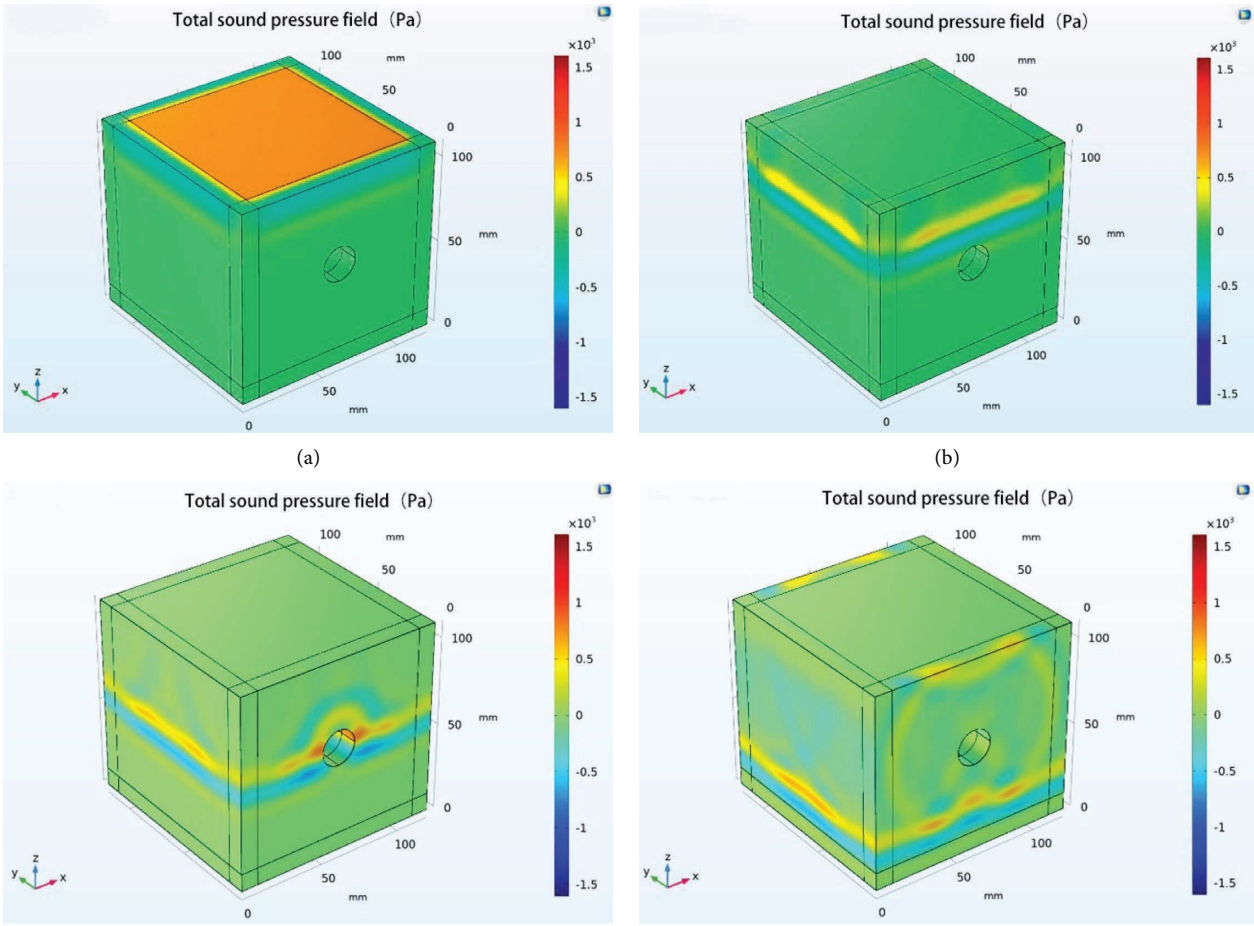

Figure 10: Sound pressure snapshot of 20 mm hole model at different times. (a) 12 μs, (b) 23 μs, (c) 33 μs, and (d) 48 μs.

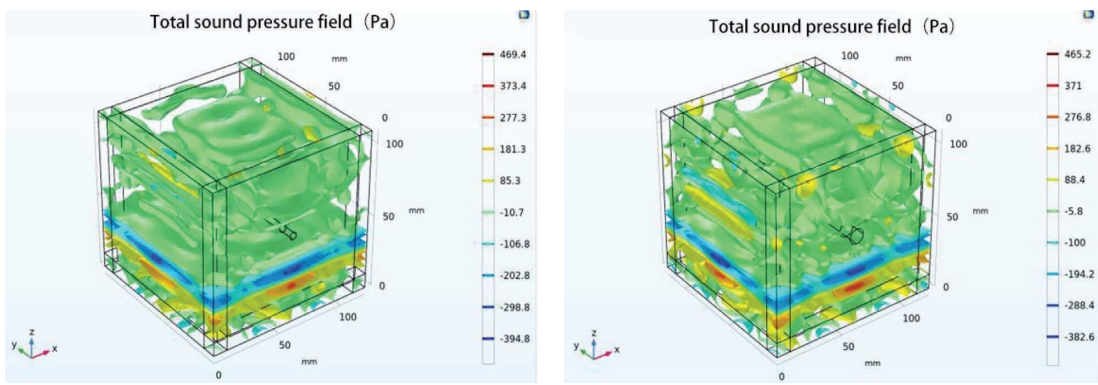

Figure 11: Continued.

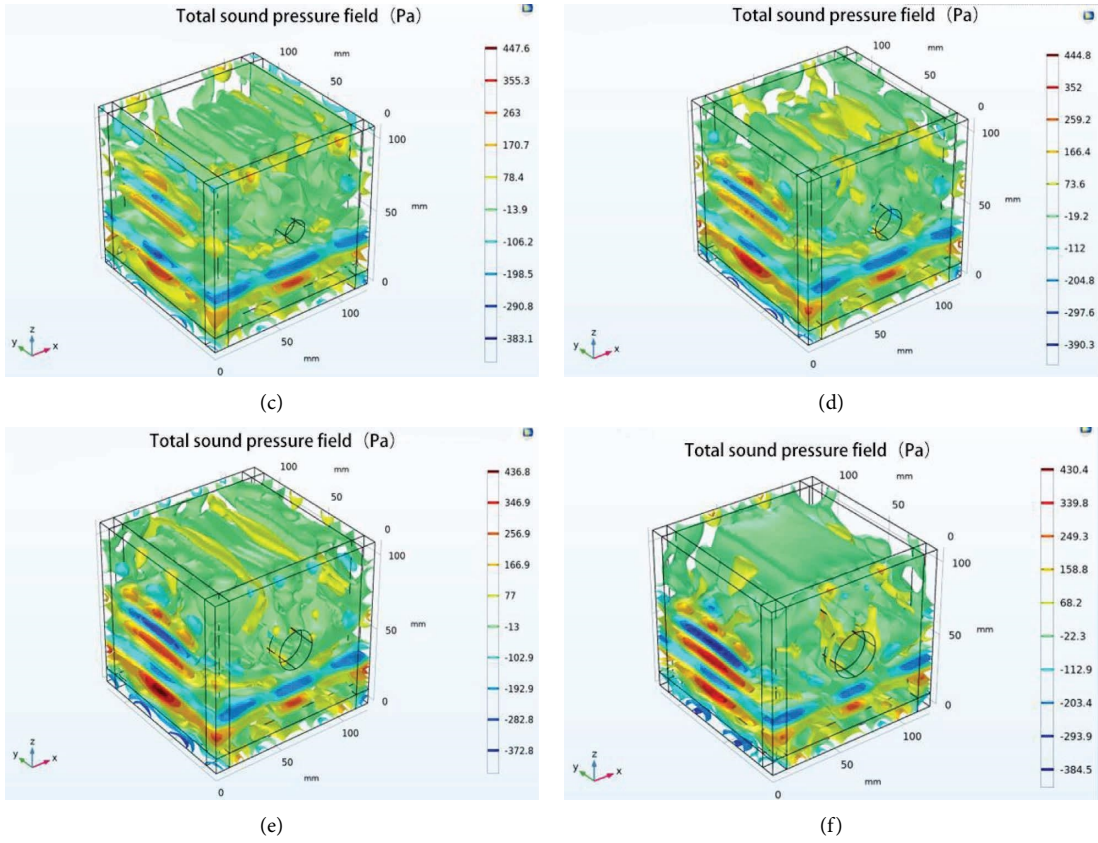

Figure 11: Schematic diagram of the acoustic pressure isosurface at 70 μs for different hole size models. (a) 5 mm, (b) 10 mm, (c) 15 mm, (d) 20 mm, (e) 25 mm, and (f) 30 mm.

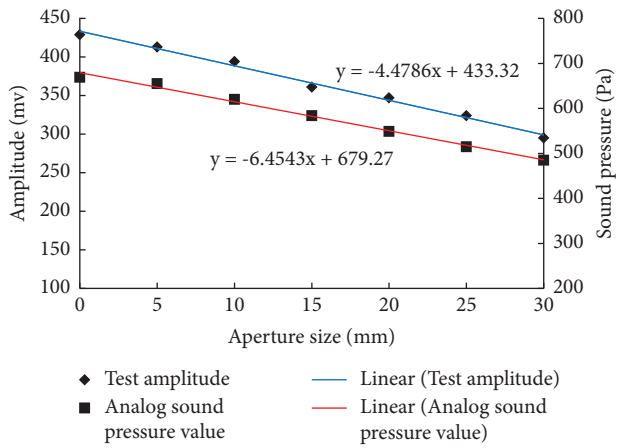

Figure 12: Relationship between the acoustic parameters and aperture size of the 100 mm × 100 mm × 100 mm model.

verified with the actual wave velocity value. As can be seen from Figure 13 and Table 5, the expected trend of the wave velocity value obtained through the SVR prediction model is consistent with the actual wave velocity value, and the training set of the model and the correlation coefficient of the testing machine are both above 0.99, which can be used as a wave velocity dataset to supplement more aperture size test block models.

5.2. Prediction of Rock Pore Size. ANN is a mathematical model for simulating the activity of artificial neurons [23–25]. It is an information processing system established based on imitating the structure and function of brain neural networks. ANN consists of an input layer, a hidden layer, and an output layer. Each layer is composed of several neurons. According to the available information data, repeated training is conducted to gradually adjust the

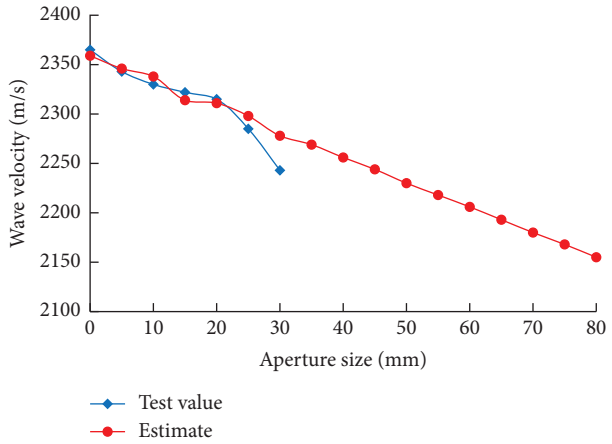

Figure 13: Predicted values and actual values of wave velocities in different pore sizes of the 100 mm × 100 mm × 100 mm model.

Table 5: Acoustic parameter enhancement dataset for different model sizes.

Rock specimen dimension (mm)	Aperture dimension (mm)	Experiment amplitude (mv)	Simulation sound pressure value (Pa)	Wave velocity (m/s)	SVR-predicted wave velocity (m/s)
100	0	429	669	2365	2359
100	5	413	655	2343	2346
100	10	394	620	2330	2338
100	15	361	585	2322	2314
100	20	347	549	2315	2311
100	25	324	515	2285	2298
100	30	295	485	2243	2278
100	35	277	453	—	2269
100	40	254	421	—	2256
100	45	232	389	—	2244
100	50	209	357	—	2230
100	55	187	324	—	2218
100	60	165	292	—	2206
100	65	142	260	—	2193
100	70	120	227	—	2180
100	75	97	195	—	2168
100	80	75	163	—	2155

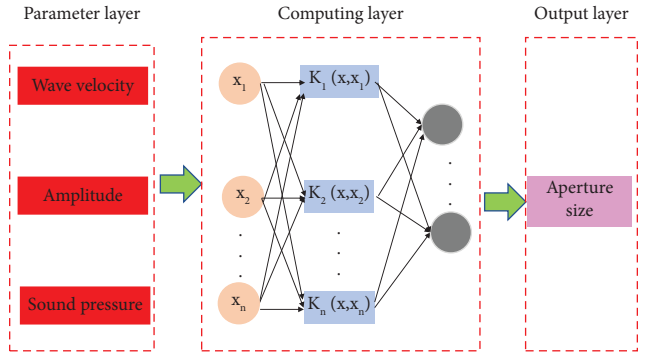

Figure 14: Diagram of the neural network model.

connection weight method between neurons to simulate the relationship between the output layer and the input layer. The number of hidden layers in a network structure and the number of neurons in each hidden layer impact the model's prediction performance. In this paper, the ANN model adopts two layers of hidden layers and takes the amplitude, wave velocity, and pressure as the input layer of the structure and the pore size contained in the rock as the output layer.

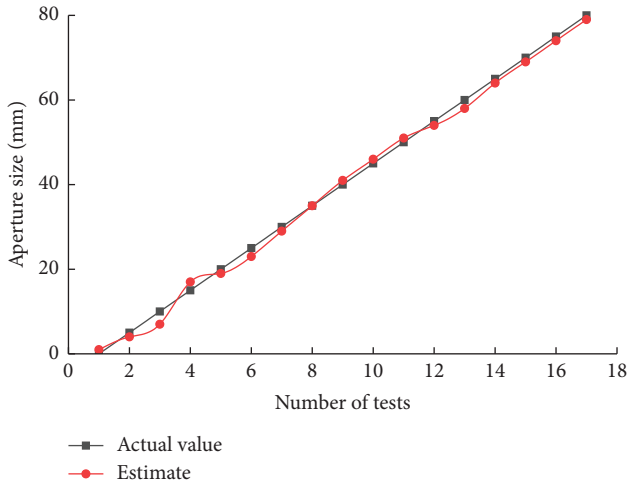

Figure 15: 100 mm × 100 mm × 100 mm model.

The structural units in the middle layer are 12 and 8 units, respectively, as shown in Figure 14.

As can be seen from Figure 15, using the ANN prediction model to predict the aperture size has a small error, which is consistent with the actual value, and the prediction curve almost coincides with the solid angle. Therefore, the model can predict the aperture size, and the prediction results are promising.

6. Conclusions

In this paper, ultrasonic testing was conducted on rocks with different apertures, and the influence of other gaps on ultrasonic parameters was analysed. The characteristics of ultrasonic pressure changes under different apertures were studied using numerical calculation methods. A method based on ANN to predict the rock pore size was proposed. The following are the conclusions drawn from the results:

(1) With the increase in the pore diameter, the longitudinal wave velocity of the rock with holes presents a downward trend, the amplitude of the first wave presents a negative linear correlation, and the attenuation coefficient presents a positive correlation. The difference in the longitudinal wave velocity, amplitude, and attenuation coefficient between the rock with holes and intact rock shows an increasing trend. The ultrasonic attenuation increases, and the rock integrity significantly decreases.

(2) To analyze the propagation patterns and acoustic field distribution characteristics of ultrasonic waves in porous rocks, the article constructs ultrasonic simulation models featuring a range of pore sizes. These models can systematically study the effects of different pore dimensions on wave behavior and field distribution. The transmission boundary acoustic pressure is negatively correlated with the pore size, and the reduction rate of the acoustic pressure amplitude is positively linearly correlated with the pore size. The propagation of ultrasonic waves in porous rocks is divided into three stages, with significant ultrasonic reflection, diffraction, and scattering phenomena occurring and considerable attenuation of acoustic pressure

(3) Based on the ultrasonic amplitude, wave velocity, and sound pressure, experimental and numerical results are analysed, and the SVR algorithm is used to enhance the prediction samples. A method for predicting rock pore size based on ANN is proposed, which inversely predicts the rock pore size with high prediction accuracy.

Data Availability

All data in this study are available from the corresponding author upon reasonable request.

Conflicts of Interest

The authors declare that they have no conflicts of interest that could have appeared to influence the work reported in this paper.

Acknowledgments

This work was supported by the Shandong Natural Science Foundation (Grant/Award nos. ZR2021ME209 and ZR2022QE251), the China Postdoctoral Science Foundation (Grant/Award no. 2022M721943), the 2023 Annual Higher Education Scientific Research Planning Project of the China Association of Higher Education (Grant/Award no. 23BR0210), and the Jiangxi Province Science Funds for Distinguished Young Youths (Grant no. 20212ACB214005).

References

[1] K. R. Hong and H. H. Feng, "Development and thinking of tunnels and underground engineering in China in recent 2 years (from 2019 to 2020)," *Tunnel Construction*, vol. 41, no. 8, pp. 1259–1280, 2021.

[2] W. Lu, L. X. Meng, S. C. Li et al., "Study on progressive failure behavior and mechanical properties of tunnel arch support structures," *Tunnelling and Underground Space Technology*, vol. 140, Article ID 105285, 2023.

[3] W. Lu and H. Sun, "Study on support characteristic curve of primary support structures in underground excavation considering bond-slip behavior," *Advances in Structural Engineering*, vol. 24, no. 3, pp. 497–508, 2021.

[4] G. Vasconcelos, P. B. Lourenço, C. A. S. Alves, and J. Pamplona, "Ultrasonic evaluation of the physical and mechanical properties of granites," *Ultrasonics*, vol. 48, no. 5, pp. 453–466, 2008.

[5] X. Chen, D. R. Schmitt, J. A. Kessler, J. Evans, and R. Kofman, "Empirical relations between ultrasonic P-wave velocity porosity and uniaxial compressive strength," *CSEG Recoder*, vol. 40, no. 5, pp. 24–29, 2015.

[6] A. G. Rafek, A. S. Serasa, L. K. Ern, and G. T. Lai, "Use of ultrasonic velocity travel time to estimate uniaxial compressive strength of granite and schist in Malaysia," *Sains Malaysiana*, vol. 45, no. 2, pp. 185–193, 2016.

[7] K. Naderi and T. Babadagli, "Influence of intensity and frequency of ultrasonic waves on capillary interaction and oil

recovery from different rock types," *Ultrasonics Sonochemistry*, vol. 17, no. 3, pp. 500–508, 2010.

[8] C. McCann and J. Sothcott, "Sonic to ultrasonic Q of sandstones and limestones: laboratory measurements at in situ pressures," *Geophysics*, vol. 74, no. 2, pp. WA93–WA101, 2009.

[9] Z. Zhao, H. Liu, X. J. Gao, and Y. Feng, "Meso-macro damage deterioration of weakly cemented red sandstone under the coupling effect of high-humidity and uniaxial loading," *Engineering Failure Analysis*, vol. 143, Article ID 106911, 2023.

[10] Z. Zhao, W. Sun, S. J. Chen, D. Yin, H. Liu, and B. Chen, "Determination of critical criterion of tensile-shear failure in Brazilian disc based on theoretical analysis and meso-macro numerical simulation," *Computers and Geotechnics*, vol. 134, Article ID 104096, 2021.

[11] L. Adam, K. van Wijk, T. Otheim, and M. Batzle, "Changes in elastic wave velocity and rock microstructure due to basalt-CO_2-water reactions," *Journal of Geophysical Research: Solid Earth*, vol. 118, no. 8, pp. 4039–4047, 2013.

[12] J. Ruedrich, C. Knell, J. Enseleit, Y. Rieffel, and S. Siegesmund, "Stability assessment of marble statuaries of the Schlossbrücke (Berlin, Germany) based on rock strength measurements and ultrasonic wave velocities," *Environmental Earth Sciences*, vol. 69, no. 4, pp. 1451–1469, 2013.

[13] M. Abdelhedi, M. Aloui, T. Mnif, and C. Abbes, "Ultrasonic velocity as a tool for mechanical and physical parameters prediction within carbonate rocks," *Geomechanics and Engineering*, vol. 13, no. 3, pp. 371–384, 2017.

[14] C. Cerrillo, A. Jiménez, M. Rufo, J. Paniagua, and F. T. Pachón, "New contributions to granite characterization by ultrasonic testing," *Ultrasonics*, vol. 54, no. 1, pp. 156–167, 2014.

[15] W. S. Wang, G. S. Cao, Y. Li et al., "Experimental study of dynamic characteristics of tailings with different reconsolidation degrees after liquefaction," *Frontiers in Earth Science*, vol. 10, Article ID 876401, 2022.

[16] Y. Liu, L. Qiao, Y. Li, G. D. Ma, A. M. Golosov, and F. Gong, "Ultrasonic spectrum analysis of granite damage evolution based on dry-coupled ultrasonic monitoring technology," *Advances in Civil Engineering*, vol. 2020, Article ID 8881800, 13 pages, 2020.

[17] Z. C. Nie, K. Wang, M. J. Zhao, and X. Sun, "Characterization of contact-type defects in mortar using a nonlinear ultrasonic method," *Advances in Materials Science and Engineering*, vol. 2020, Article ID 8832934, 11 pages, 2020.

[18] C. Kurtuluş, M. Üçkardeş, U. Sarı, and Ş. Onur Güner, "Experimental studies in wave propagation across a jointed rock mass," *Bulletin of Engineering Geology and the Environment*, vol. 71, no. 2, pp. 231–234, 2012.

[19] G. T. Baechle, R. Weger, and G. P. Eberli, "The role of macroporosity and microporosity in constraining uncertainties and in relating velocity to permeability in carbonate rocks," in *Proceedings of the SEG Annual Meeting*, OnePetro, Richardson, TX, USA, January 2004.

[20] M. Kumar and D. Han, "Pore shape effect on elastic properties of carbonate rocks," in *Proceedings of the SEG Annual Meeting*, OnePetro, Richardson, TX, USA, January 2005.

[21] G. Hevin, O. Abraham, H. A. Pedersen, and M. Campillo, "Characterization of surface cracks with Rayleigh waves: a numerical model," *NDT & E International*, vol. 31, no. 4, pp. 289–297, 1998.

[22] B. Keshtegar, M. L. Nehdi, N. T. Trung, and R. Kolahchi, "Predicting load capacity of shear walls using SVR–RSM model," *Applied Soft Computing*, vol. 112, Article ID 107739, 2021.

[23] M. Zarringol and H. T. Thai, "Prediction of the load-shortening curve of CFST columns using ANN-based models," *Journal of Building Engineering*, vol. 51, Article ID 104279, 2022.

[24] A. Ketsakorn, K. Samana, and P. Sripaiboonkij, "The artificial neural network (ANN) model for predicting the preventive behaviors toward dust exposure among stone crushing mill workers," *Safety and Health at Work*, vol. 13, p. S87, 2022.

[25] K. Peng, J. Zeng, D. J. Armaghani, M. Hasanipanah, and Q. Chen, "A novel combination of gradient boosted tree and optimized ANN models for forecasting ground vibration due to quarry blasting," *Natural Resources Research*, vol. 30, no. 6, pp. 4657–4671, 2021.